energies

MDPI

Article

Optimal Estimation of Under-Frequency Load Shedding Scheme Parameters by Considering Virtual Inertia Injection

Santiago Bustamante-Mesa [1,2], Jorge W. Gonzalez-Sanchez [2], Sergio D. Saldarriaga-Zuluaga [1], Jesús M. López-Lezama [3,*] and Nicolás Muñoz-Galeano [3]

[1] Departamento de Eléctrica, Facultad de Ingenieria, Institución Universitaria Pascual Bravo, Calle 73 No. 73A-226, Medellín 050036, Colombia; san.bustamante@pascualbravo.edu.co (S.B.-M.); s.saldarriagazu@pascualbravo.edu.co (S.D.S.-Z.)
[2] Grupo de Investigación Transmisión y Distribución de Energía Eléctrica (TyD), Universidad Pontificia Bolivariana, Medellín 050031, Colombia; jorgew.gonzalez@upb.edu.co
[3] Research Group on Efficient Energy Management (GIMEL), Department of Electrical Engineering, Universidad de Antioquia (UdeA), Calle 70 No. 52-21, Medellín 050010, Colombia; nicolas.munoz@udea.edu.co
* Correspondence: jmaria.lopez@udea.edu.co

Abstract: Under-frequency load shedding (UFLS) schemes are the latest safety measures applied for safeguarding the integrity of the grid against abrupt frequency imbalances. The overall inertia of electrical power systems is expected to decrease with an increased penetration of renewable energy as well as elements connected through power electronic interfaces. However, voltage source converter-based high voltage direct current (VSC-HVDC) links can provide virtual inertia through a control loop that allows for a reaction to occur at certain frequency fluctuations. This paper evaluates a UFLS scheme that considers the injection of virtual inertia through a VSC-HVDC link. A genetic algorithm (GA) is used to determine the location of the UFLS relays, the activation threshold of each stage, the delay time and the percentage of load shedding at each stage. It was found that the virtual inertia causes the nadir to delay and sometimes reach a greater depth. Furthermore, the implemented GA approximates the frequency response to the limits set with the constraints, reducing the load shedding but achieving a steeper nadir and a lower steady-state frequency level than traditional UFLS. The simulations were performed using the IEEE 39-bus test system.

Keywords: inertia; virtual power plants; genetic algorithms; VSC-HVDC; UFLS

check for updates

Citation: Bustamante-Mesa, S.; Gonzalez-Sanchez, J.W.; Saldarriaga-Zuluaga, S.D.; López-Lezama J.M.; Muñoz-Galeano, N. Optimal Estimation of Under-Frequency Load Shedding Scheme Parameters by Considering Virtual Inertia Injection. *Energies* **2024**, *17*, 279. https://doi.org/10.3390/en17020279

Academic Editor: Ahmed Abu-Siada

Received: 16 November 2023
Revised: 31 December 2023
Accepted: 1 January 2024
Published: 5 January 2024

Copyright: © 2024 by the authors. Licensee MDPI, Basel, Switzerland. This article is an open access article distributed under the terms and conditions of the Creative Commons Attribution (CC BY) license (https://creativecommons.org/licenses/by/4.0/).

1. Introduction

In the context of the increasing integration of renewable energy sources interfaced with grid-connected inverters and the evolution toward more decentralized and flexible power systems, grid security and stability have become crucial challenges [1,2]. Frequency deviations are among the most critical threats in power systems. Frequency may experience significant deviations due to events such as generator tripping or the variability of intermittent renewable generation [3]. Since the frequency is essentially the speed of the power system, it can be understood as an indicator of the balance between generation and demand [4], which increases when generation is greater than demand (accelerated system) and decreases when demand exceeds generation (decelerated system) [5].

The overall stability of electrical systems is often closely related to their inertia levels. With the massive penetration of elements connected through power electronics, the total synchronous inertia of the system tends to decrease; therefore, systems become more vulnerable to reach unstable operating points in the presence of any major disturbance in the power system. However, the ability of certain devices such as voltage source converter-based high voltage direct current (VSC-HVDC) schemes to provide virtual inertia through various control strategies has been proven.

Power systems are constantly subjected to fluctuations in power levels due to imbalances between generation and demand, caused by events such as the loss of generating units or the sudden connection of large loads. These abrupt changes affect the frequency, which may lead to further imbalances and eventually to a blackout. Under-frequency load shedding (UFLS) schemes are used to prevent the frequency from reaching critical levels. These schemes are designed to disconnect load in a controlled manner during grid emergencies. Their main objective is to re-establish the generation–demand balance by disconnecting a part of the load.

The conventional implementation of UFLS presents limitations since it can lead to excessive or insufficient load disconnection, which worsens the frequency behavior. This problem expands proportionally to the increase in under-frequency relay (UFR) units, since the parameters to be defined increase and the problem of sizing the UFLS scheme becomes more complex [6]. Because UFLS schemes based on computational techniques are focused on optimizing their performance, they are often considered superior or better performing [7].

Several authors have focused their efforts in the area of UFLS and particularly in the use of computational techniques for their operation, such is the case of [8], which presents a multi-objective approach based on particle swarm optimization (PSO) to determine both the magnitude of the load shedding and the delay of each load shedding stage. In [7], an adaptive strategy is designed based on the execution of neural networks and the study of the transient stability of the network. In [9], the authors consider as input neurons the total generation, the total system load, the hydraulic generation reserve and the frequency reduction rate for the implementation of a GA that seeks to minimize the load shedding. A UFLS protection system that minimizes load shedding based on the detection of frequency excursions is presented in [10]. The problem is developed with mixed-integer linear programming optimization and solved for various stochastic scenarios. The design of a fuzzy logic-based UFLS controller for a system operating in island mode with a single generator is explained in [11]. In [12], the authors present a UFLS that bases its operation on a neuro-fuzzy method for determining the amount of load to be shed to avoid cascading outages. In [13], the authors present a UFLS scheme that aims to minimize load shedding using a grasshopper optimization algorithm while prioritizing low-frequency oscillations at all stages of the scheme. Some examples of research dealing with UFLS schemes that use mixed-integer linear programming are presented in [10,14,15]. In all cases, the aim is to minimize load shedding and ensure the stability of the system. In [16], the authors introduce a chance-constrained approach to choose feeders, ensuring a mathematically verified disconnection of the necessary load volume with a predefined probability. It explicitly accounts for the correlation in net load predictions across feeders, acknowledging the high interdependence in DG power output uncertainties due to shared meteorological conditions within the network. A static voltage stability-based zoning mechanism using Fisher–Jenks' natural breaks algorithm is proposed in [17]. The zoning approach resorts to the reactive power margin of buses to cluster them into several zones. Then, UFLS schemes are devised for each zone stemming from their independent frequency response characteristics, particularly RoCoF. In [18], a hierarchical UFLS scheme for centralized real-time decision making and decentralized real-time control is proposed for interconnected power systems. A thorough review of the UFLS schemes available in the literature is presented in [19].

Many of the UFLS schemes mentioned above simplify the problem of their configuration by making the parameters of each of the UFR unit the same, ignoring aspects such as the magnitude of the load to which they are associated, the proximity to the generation nodes, etc. This simplification results in inadequate estimates of the load shedding block, which may lead to incorrect frequency recoveries, or in some cases, to over-frequencies. On the other hand, the methodologies presented in [20,21] simplify the optimization problem by ignoring several of the parameters of the UFLS scheme by considering only the amount of the load shedding, which limits the solution of the problem and may lead to erroneous

estimates of its parameters. These parameters are taken into account in [6]; however, such methodology does not estimate which UFR locations would have the greatest impact on the behavior of the UFLS scheme.

The main objective of this paper is to optimally calculate the configuration of the UFLS scheme. In this case, the parameters of each of the UFR units are estimated (load shedding block size, frequency threshold and time delay for each stage) and six stages defined by the activation frequency thresholds are considered. In addition, the optimal location of the UFR units and the virtual inertia contribution via a VSC-HVDC scheme are determined. The objective function described for the optimization problem seeks to minimize the total amount of load shedding. To summarize, the main features and contributions of this paper are as follows:

- A UFLS scheme is proposed that considers the injection of virtual inertia using a VSC-HVDC link;
- The optimal location of the UFL relays, the activation threshold of each stage as well as the delay time and percentage of load shedding at each stage are determined through a GA.

The remainder of the paper is organized as follows. Section 2 presents a brief description of the virtual inertia provided by the VSC-HVDC link. Section 3 presents the operating principles of the traditional UFLS scheme. Section 4 presents in detail the characteristics of the UFLS scheme proposed in this research work and the methodology used to optimize its parameters. Section 5 describes the test system used to corroborate the performance of the scheme and analyzes the results of the proposed case studies. Finally, Section 6 presents the main observations and conclusions.

2. Virtual Inertia

In an electrical system, the frequency reflects the balance between generation and load by showing how the system accelerates or decelerates when faced with imbalances of these two variables. Thus, in the event of a large active power imbalance, caused, for example, by the loss of a generation unit, the frequency should decrease since the system would be overloaded, with loads predominating over generation. When a frequency unbalance occurs, it is usually taken care of instantaneously by the natural inertia of the system, i.e., by releasing or absorbing energy in the rolling masses of the rotating machines. Generator controllers inject more power from reserves. The Automatic Generator Control (AGC) is activated and, finally, the tertiary control is activated [22].

With the injection of power from sources that do not provide an inertial response, the first stage of response to frequency disturbances is impaired and subsequent stages are affected. This makes it necessary to implement, in a controlled manner, an inertial response by the power electronics interfaces to maintain a safe and reliable operation of the power system.

2.1. Inertia Constant and Oscillation Equation

The inertia constant of a rotating system H or of a single generator H_i is used to define the energy stored in its rotating mass E_{c0}. This definition consists of the time (in seconds) it would take to replace this stored energy when operating at nominal mechanical speed ω_{sm} and at nominal apparent power S_{base}. The general inertia of the system is presented in Equation (1) [23]:

$$H = \frac{E_{c0}}{S_{base}} = \frac{J\omega_{sm}^2}{2S_{base}} \quad (1)$$

where J is the total moment of inertia in kg·m^2, ω_{sm} is the angular velocity of the system expressed in rad/s and S_{base} is the selected base power in MVA.

The relationship between the frequency f_i and the power unbalance ΔP_i at the terminals of generator i can be expressed using Equation (2):

$$\frac{2Hi}{f_n} \cdot \frac{df_i}{dt} = p_{m,i} - p_{e,i} = \Delta p_i \qquad i = 1, 2, \ldots, N \tag{2}$$

where $p_{m,i}$ is the mechanical power of the turbine in p.u., $p_{e,i}$ is the electric power in p.u., Δp_i represents the power imbalance between generation and load in p.u., H_i is the inertia constant in seconds, f_i is the frequency seen by the element i in Hz, f_n is the nominal frequency of the system in Hz and df/dt is the rate of change of the frequency in Hz/s.

If the instant at which the perturbation occurs is known $t = t_0$, as well as the size of the power imbalance $\Delta p_i(t_0)$ and the rate of change of the frequency df_i/dt, then the inertia delivered by the generator can be calculated using Equation (3):

$$\hat{H}_i = \frac{\Delta p_i(t_0) f_n}{2 \frac{df_i}{dt}|_{t=t_0}} \tag{3}$$

Equation (3) will only be valid some time after the perturbation, before other factors affect the dynamic behavior of the system [22]. Since the RoCoF is the rate of change of frequency, it can be estimated by making consecutive measurements to determine the slope with Equation (4):

$$\frac{df_i}{dt}|_{t=t_0} \cong \frac{f_i(t_0^+) - f_i(t_0^-)}{t_0^+ - t_0^-} \tag{4}$$

where $f_i(t_0^+)$ and $f_i(t_0^-)$ correspond to the frequency data taken at t_0^+ and t_0^-, respectively.

2.2. Synthetic Inertia

Conventional VSC-HVDC systems do not provide frequency response naturally and automatically. In this case, it is necessary to implement additional control loops to enable communication between the grid frequency and the generation output to enable frequency response in VSC-HVDC systems during disturbances in the AC system. For this purpose, ref. [24] describes two strategies for inertia delivery via the VSC-HVDC links to the power grid to face frequency disturbances or active power imbalances: one-shot RoCoF control and continuous RoCoF control.

Continuous RoCoF control employs a measurement of the instantaneous RoCoF value on the grid side, which gives it high adaptability but requires more complex control to filter out harmonics, as the instantaneous RoCoF measurement can introduce a noise amplifying effect. On the other hand, single-action RoCoF control is based only on the initial RoCoF value, which makes it simpler and more predictable, but not as adaptive as continuous RoCoF control [25].

Once the value of the frequency is known, it can be derived with respect to time, and due to the noisy nature of this output, it must be filtered and then multiplied by a gain called synthetic inertia constant. Equation (5) represents this behavior:

$$\Delta p = 2H_{syn} \cdot \frac{df_{sys}}{dt} \tag{5}$$

where Δp represents the inertial active power of the machine, H_{syn} is the inertial of the machine and f_{sys} is the frequency of the system.

The energy delivered in the form of inertia may come from various sources such as the DC link capacitor [26], from the kinetic energy stored in the rolling masses of the turbines [27] or from both elements [28]. Figure 1 depicts the simplified inertia control loop for calculating Δp and performing frequency regulation using the VSC-HVDC link [25].

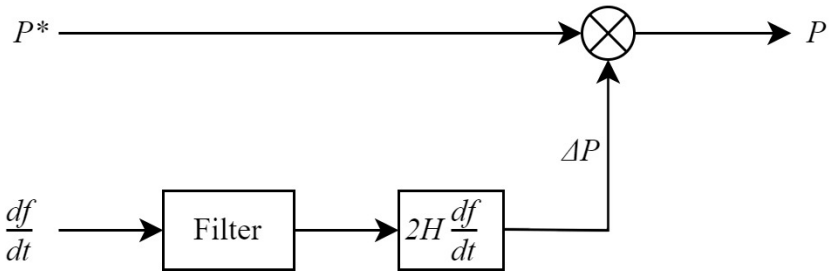

Figure 1. Generic block diagram of inertial control on VSC-HVDC links.

The strategy used in the simulations consists of adding an inertial control loop to the DC–AC converter of the VSC-HVDC link to modify the DC voltage proportionally to the frequency variations of the network. On the other hand, for the rectifier side to deliver the required power, a PV control mode is established in which the control setpoint is to maintain the DC bus voltage at 1.0 p.u., forcing the system to increase the power from the AC network formed by the wind turbines and in the direction of the test network.

3. Under-Frequency Load Shedding Scheme

The conventional implementation of UFLS schemes focuses on setting the parameter values of all the units or relays installed in the power system. These units are mainly characterized by four parameters, as shown in Figure 2: (i) the number of stages N_s or steps in which the UFLS will disconnect the locally connected load, (ii) the size of the load ΔP that will be shed in every stage, (iii) the frequency threshold f_T that activates each of the load shedding stages and (iv) the delay time *td* between the activation of consecutive steps [6].

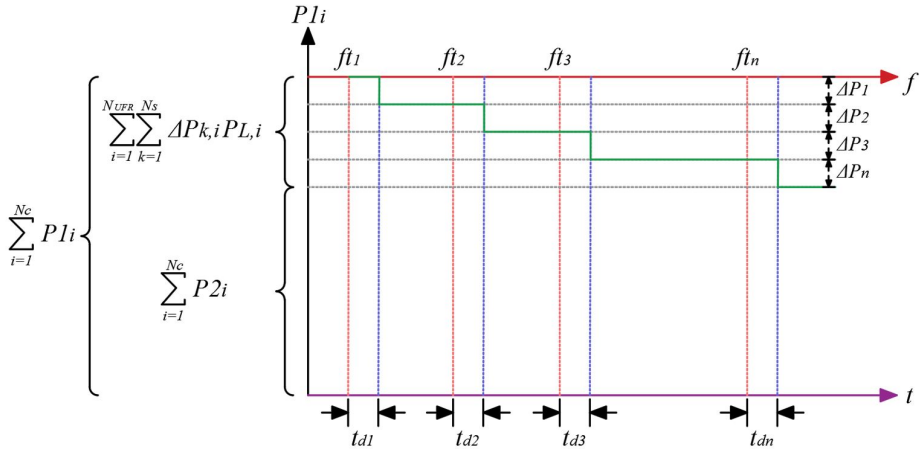

Figure 2. Basic parameters of the UFLS scheme.

If the power system is considered to have a given number of UFR units installed N_{UFR}, the settings of the *i*-th unit can be described mathematically by Equations (6)–(8):

$$\Delta P_i = [\Delta P_{1,i}\ \Delta P_{2,i}\ \ldots\ \Delta P_{k,i}\ \ldots\ \Delta P_{N_s,i}]_{\cdot N_s} \tag{6}$$

$$F_i = [f_{T1,i}\ f_{T2,i}\ \ldots\ f_{Tk,i}\ \ldots\ f_{TN_s,i}]_{\cdot N_s} \tag{7}$$

$$T_i = [t_{d1,i}\ t_{d2,i}\ \ldots\ t_{dk,i}\ \ldots\ t_{dN_s,i}]_{\cdot N_s} \tag{8}$$

where $\Delta P_{k,i}$ defines the size of the load shedding block, $f_{Tk,i}$ represents the frequency threshold and $t_{dk,i}$ is the intentional time delay of the *k*-th stage in the *i*-th relay. The complexity of calculating the four configurations of each relay increases as more units are

installed in the power system. This is because $3 \cdot Ns$ parameters need to be calculated for each relay; therefore, the total number of parameters to be calculated in the power system is $(3Ns + 1) \cdot N_{UFR}$.

For a proper UFLS operation, it is necessary to consider a set of configurations that include the dynamics of the power system. When implementing the UFLS scheme, both the maximum frequency deviation Δ_f and the depth of the frequency response f_{nadir} must be limited to protect the generating units from prolonged high- or low-frequency conditions. Therefore, it is essential to coordinate the UFLS scheme with the low-frequency protection of the generating units. Additionally, the UFLS scheme should account for a reasonable margin between the nominal frequency f_0 and the first-stage frequency threshold f_{T1} to prevent the activation of UFRs under non-emergency frequency conditions [6].

4. Optimal Under-Frequency Load Shedding Scheme Using a GA

4.1. Mathematical Approach

The frequency metrics during primary frequency response (typically occurring within the first 10–30 s after a frequency event) are represented by the time t_{min} at which the frequency reaches its maximum depth, referred to as the minimum instantaneous frequency f_{min} or the lowest point of frequency f_{nadir}, and the value at which the frequency stabilizes, known as the steady-state frequency f_{ss} [6]. After a system frequency disturbance, both inertia and the action of the UFLS directly influence the frequency response metrics. The metrics are as follows: (1) the total amount of load shedding, (2) the frequency threshold, and (3) the impact of time delay on the values of f_{min} and t_{min}. The total amount of load shedding primarily determines the level at which the frequency will stabilize f_{ss}. Therefore, the UFLS parameters (N_s, ΔP, f_T and t_d), and even the placement of the UFRs, can be considered as frequency control variables to formulate the UFLS as an optimization problem.

The UFLS scheme is formulated as a mathematical optimization problem that aims to minimize the amount of shed load during a frequency event by obtaining the optimal parameters for each of the relays that constitute it. In this case, the minimization of load shedding was used as the objective function by considering: (1) the percentage of load to be shed at each stage, (2) the activation threshold for each stage, (3) the intentional time delay between each of the stages and (4) the placement of each of the relays, i.e., whether a relay is activated or not or if it is considered within the scheme design. If these parameters of the UFRs are considered to solve the optimization problem, the vector of control variables X_{FC} can be represented using Equations (9) and (10):

$$X_{FC} = [X_1\ X_2\ \ldots\ X_i\ \ldots\ X_{N_{UFR}}] \tag{9}$$

$$X_i = [UFR_i\ \Delta P_i\ F_i\ T_i] \cdot N_s \quad \forall_i = 1, 2, \ldots, N_{UFR} \tag{10}$$

where X_i represents the vector of parameters for each relay. If the relay is in state zero, it indicates that it is not being considered or is turned off. The total number of variables is defined by Equation (11):

$$N = 3 \cdot N_{UFR} \cdot N_s + N_{UFR} \tag{11}$$

The sum of N_{UFR} represents the status of each of the relays within the set of solutions. Thus, the algorithm can decide whether to activate a specific relay or not (i.e., whether it is convenient to consider it within the set of solution parameters). Based on the resulting state of each X_i, the location of the relays to be considered for the optimal UFLS scheme can be determined.

Each of the parameters has operational constraints defined by the grid operator. Equation (12) represents the maximum and minimum values of power that each load can shed. The minimum and maximum frequency at which each stage is activated is

represented in Equation (13). The maximum and minimum values of the time delay between each stage are represented by Equation (14).

$$\Delta P_{min} < \Delta Pshed_i < \Delta P_{max} \quad \forall_i = 1, 2, \ldots, N_{UFR} \tag{12}$$

$$F_{min} < Fset_i < F_{max} \quad \forall_i = 1, 2, \ldots, N_{UFR} \tag{13}$$

$$T_{min} < Tdel_i < T_{max} \quad \forall_i = 1, 2, \ldots, N_{UFR} \tag{14}$$

where $Fset_i$ corresponds to the frequency threshold at which the i-th stage of the relay will be activated; $Tdel_i$ is the delay time before the i-th stage of the relay begins operation and $\Delta Pshed_i$ corresponds to the value of shed power in the i-th operating stage of the UFR.

4.2. Objective Function

The objective of optimizing the UFR configuration is to minimize the total load shedding after a low-frequency disturbance. This is performed to restore the frequency within permissible values and avoid situations of overloading or underloading that may be caused by incorrect UFLS scheme configurations. The objective function is defined as the sum of all active powers disconnected by the UFRs and is expressed by Equation (15) [6]:

$$\min_x[f(X_{FC})] = \min_x[P_{LS}(X_{FC})] = \sum_{i=1}^{N_{UFR}} \sum_{k=1}^{N_sT} \Delta P_{k,i} P_{L,i} \tag{15}$$

where $P_{L,i}$ corresponds to the total active power assigned or controlled by the i-th UFR unit or relay, $\Delta P_{k,i}$ is the size of the k-th load shedding block for the i-th unit (given in per unit or percentage), N_{UFR} corresponds to the number of units that conform the UFLS scheme and N_sT represents the number of stages activated during the frequency event, so this value can be equal to or less than N_s.

The objective function can also be considered as the difference between the power demanded by the load before the event and the power after the action of the UFLS scheme, so the objective function can be rewritten using Equation (16):

$$\min_x[f(X_{FC})] = \min_x[P_{LS}(X_{FC})] = \sum_{i=1}^{N_C} P1_i - \sum_{k=1}^{N_C} P2_i \tag{16}$$

where $P1_i$ corresponds to the value of active power demanded by the i-th load of the system before a fault occurs; $P2_i$ corresponds to the value of active power demanded by the i-th load of the system after the frequency event and the corresponding operation of the UFLS scheme. Meanwhile, N_c represents the set of system loads, as shown in Figure 2.

4.3. Genetic Algorithm

Metaheuristic optimization techniques are computational methods designed to efficiently solve complex optimization problems, especially in scenarios where traditional exact algorithms struggle due to high dimensionality, nonlinearity, or non-convexity. These techniques are often inspired by natural phenomena or social behavior, and offer robustness, flexibility and adaptability [29–31].

A GA implemented in Python was used to solve the model described by Equations (6)–(16). GAs are metaheuristics that mimic the Darwinian evolutionary process, wherein the fittest individuals are more likely to transmit their traits to the next generation. GAs have been applied successfully to a variety of problems such as vulnerability assessment [32,33], protection coordination [34,35], expansion planning [36,37], etc. Furthermore, it has been demonstrated that GAs are effective in addressing the problem of UFLS scheme dimen-

sioning, as indicated in [38–40]. Figure 3 illustrates the flowchart of the implemented GA [41].

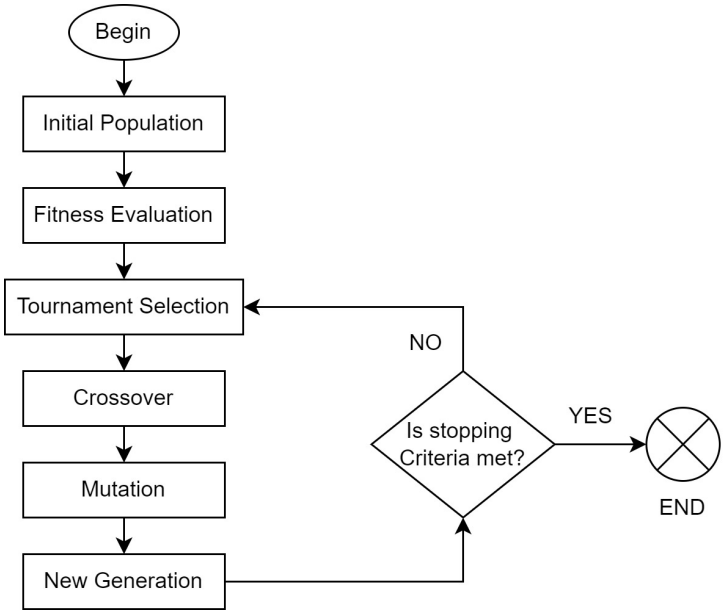

Figure 3. Flowchart of the implemented genetic algorithm (GA).

4.3.1. Initial Population

The GA begins with a set of candidate solutions as an initial population, referred to as individuals, which represent a potential solution to the optimization problem. In this case, each element of the solution vector corresponds to a configuration parameter of each UFR relay comprising the UFLS scheme. The vector's length can be determined using Equation (11). Figure 4 illustrates an example of an individual or candidate solution. In this case, the candidate solution consists of a vector that initially contains the on/off state of each UFR relay, followed by the frequency threshold values F_{set}, the time delay between each stage T_{del} and the shedding percentage for each stage Δ_{shed} for the first UFR relay. This information is then repeated for each subsequent UFR relay.

UFR 1	Fset$_{1,1}$	...	Fset$_{1,Ns}$	Tdel$_{1,1}$	...	Tdel$_{1,Ns}$	Δshed$_{1,1}$	...	Δshed$_{1,Ns}$	...	UFR$_{NUFR}$	Fset$_{NUFR,Ns}$	Tdel$_{NUFR,Ns}$	Δshed$_{NUFR,Ns}$
0	59.4	...	58.5	0	...	0.4	0	...	6.7	...	0	59	0.2	3

Figure 4. Example of an individual or candidate solution.

4.3.2. Fitness Evaluation

In GAs, fitness evaluation represents the assessment of how suitable or effective a candidate solution is based on its ability to solve the stated problem. Fitness evaluation aims to assign a numerical value to each individual in the population. The fitness function or objective function establishes the criteria by which the quality of a candidate solution is evaluated. In this case, the objective function is defined by Equation (16) and represents the difference between the system's active power before and after the implementation of the UFLS scheme. To ensure that constraints are met, the fitness function is penalized for infeasible individuals by assigning a value greater than the total system load. The most favorable candidates for a solution are those corresponding to the lowest value of the objective function.

4.3.3. Tournament Selection

After evaluating the objective function, some of the best individuals are selected to generate new potential solutions. In this case, a tournament selection technique is employed,

which involves randomly selecting two pairs of individuals and choosing the individual with the best fitness or objective function as many tournaments are conducted based on the number of individuals. The selected individuals then proceed to the subsequent stages of crossover and mutation.

4.3.4. Crossover Process

The crossover or recombination stage involves the exchange of genetic material between the parents to generate new individuals. In this particular case, the crossover occurs between two tournament winners acting as parents. Their genes are crossed at a random position within the vectors, resulting in the creation of two offspring, or two new individuals. Each offspring inherits a portion of genetic material from both parents.

4.3.5. Mutation

Mutation involves introducing small variations in the new individuals, typically carried out with a predefined probability. The objective of the mutation stage is to introduce diversification and enable the algorithm to escape from local optimal solutions. During the mutation process, one of the offspring is randomly selected with a specified probability and one of its genes is modified. In this specific case, the current value of the selected gene is randomly changed within its defined limits.

4.3.6. New Generation

After completing the processes of recombination and mutation, the population of offspring and parents is merged. Subsequently, the fitness of each individual is used to select the new population. Since the new population will be double the size of the initial one, half of the individuals are discarded, specifically those with inferior performance. In this way, a new generation is prepared for the subsequent iteration of the algorithm.

4.3.7. Stopping Criteria

In the developed GA, two termination criteria are established: a predetermined maximum number of iterations and a maximum number of iterations without improvement in the objective function. If either of these two criteria is met, the algorithm is stopped.

4.4. Co-Simulation Framework: PowerFactory + Python

The implementation of the GA was carried out through the co-simulation of two subsystems: one focused on obtaining the frequency response of the power system using DigSILENT PowerFactory and the other dedicated to iteratively solving the numerical optimization problem using Python. An illustration of such configuration is presented in Figure 5, prominently demonstrating the division between the processes carried out in the optimization software and the power systems software. The stages included in the flowchart summarizing the proposed methodology are, in descending order:

- Step 1: A vector X is defined, with the parameters of the candidate solution.
- Step 2: The space of possible values is defined for each of the genes of vector X. Thus, vectors X_{min} and X_{max} represent the limits of the parameters associated with the candidate solution.
- Step 3: The initial population is created by configuring individuals randomly.
- Step 4: The parameters of each individual are sent as configuration inputs for each of the UFRs that make up the UFLS system implemented in DigSILENT PowerFactory.
- Step 5: The inertial response control scheme of the VSC-HVDC link is activated.
- Step 6: A load flow is executed, and the total active power consumed by the system is exported to the GA in Python.
- Step 7: The initial conditions and dynamic simulation are run in DigSILENT PowerFactory, taking into account the frequency events defined in the dynamic simulation.
- Step 8: The results of the frequency time series and the total value of active power demanded by the system after UFLS action are sent to the GA in Python.

- Step 9: The objective function is evaluated by finding the difference between the total consumed active power values. If frequency violation values are evident in the frequency time series, the objective function takes a value that renders this individual unfeasible as a solution.
- Step 10: The selection tournament is conducted.
- Step 11: The individuals selected in the selection tournament are crossed over.
- Step 12: A mutation is applied to the resulting individuals from the crossover.
- Step 13: With the mutation included in the genes of the individuals, the new generation is ready to be evaluated.
- Step 14: If the stopping criteria are met, the algorithm stops, providing the solution. Otherwise, the algorithm returns to Step 4 and repeats the cycle until the stopping criteria are met.

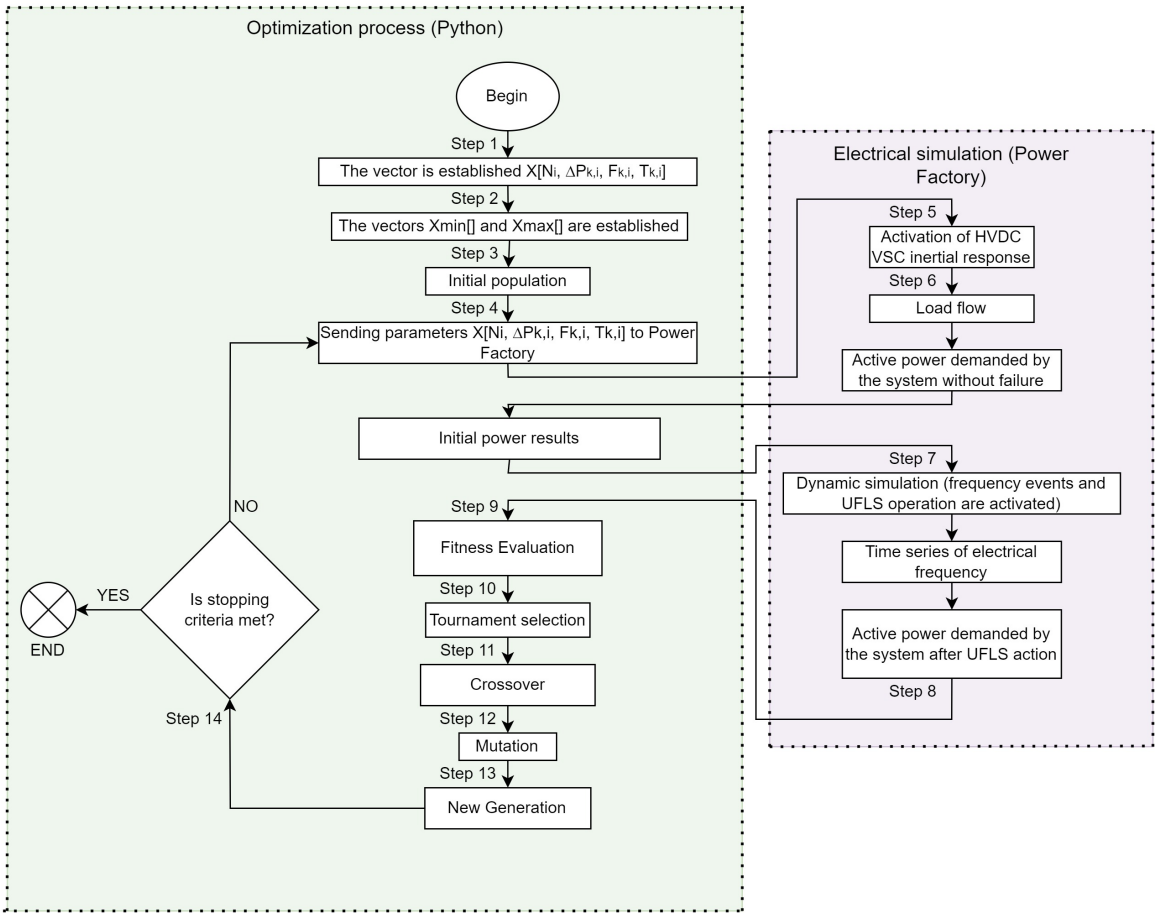

Figure 5. Co-Simulation framework for the UFLS scheme.

5. Results

This section presents the results of applying the proposed methodology to a case study using the DigSILENT PowerFactory and Python tools. Simulations are conducted on the IEEE 39-bus test system, incorporating a VSC-HVDC link with its respective control schemes for normal operation and the provision of synthetic inertia. A wind farm is connected to the test system using the highlighted blue VSC-HVDC link in Figure 6. In this system, loads are represented as constant power injections. Several authors have proposed different connection buses of HVDC links in the IEEE 39-bus test system. In [42], an HVDC link is connected to the system on bus 18, replacing the thermal generators on buses 30 and 32. In [43], a multi-terminal HVDC (HVDC MTDC) link is connected between nodes 4, 16 and 17; whereas in [44], it is connected to buses 16, 21, 22, 23 and 24. Also, in [45], buses 16 and 26 are used for the connection of an HVDC MTDC link. In this work, the HVDC

link is connected to bus 16 since it is common in the connection of several HVDC links and because this bus is usually considered as the connection point when the system is divided in two [46] or three areas [47].

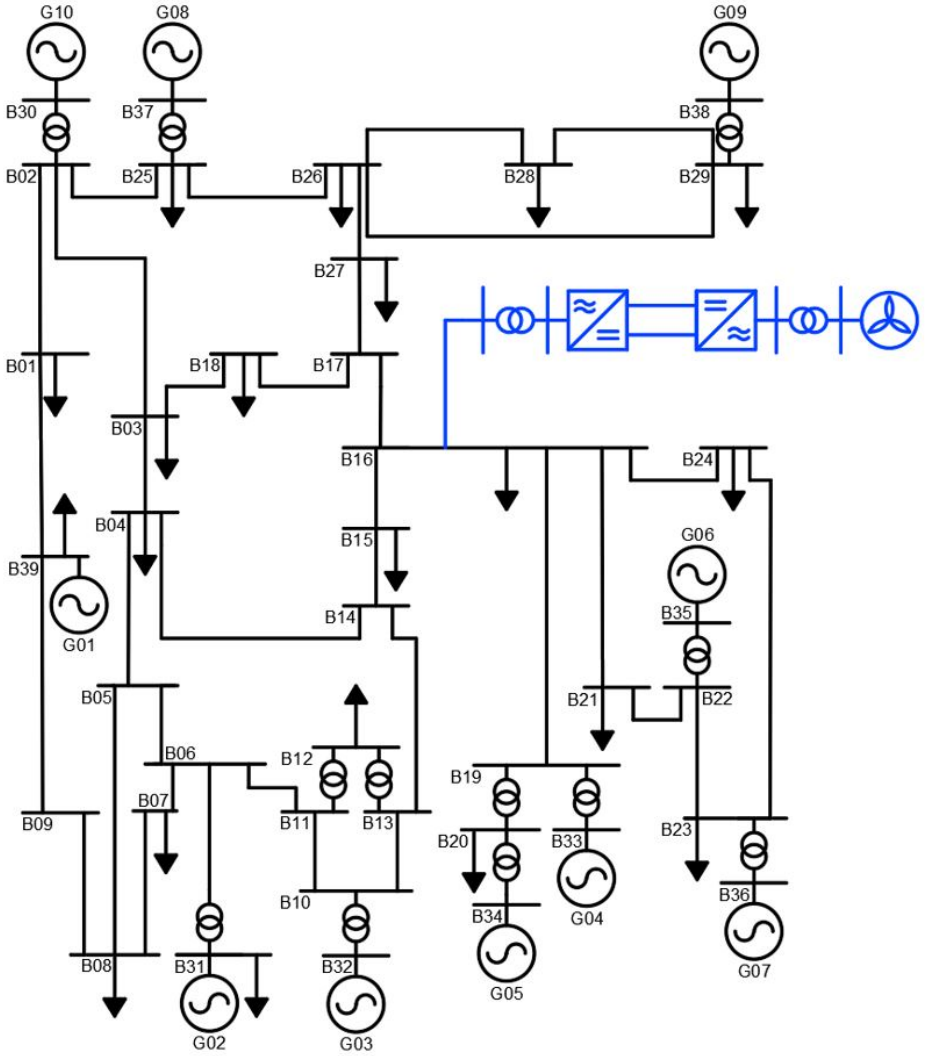

Figure 6. IEEE 39-bus test system with VSC-HVDC link.

The system consists of 39 alternating current buses, 47 transmission lines, 19 loads and 10 synchronous generators. Table 1 presents the generator dispatch parameters where G02 is the slack bus (SL) and the others are PV buses. Table 2 provides a summary of the loads comprising the system, specifying active and reactive powers. The parameters of the lines and transformers of this system can be consulted in Appendix A.

The wind farm consists of four sets of 20 wind generators each. Each generator can deliver 5.0 MW at a voltage of 0.69 kV, requiring a transformer with a transformation ratio of 0.69/33 kV. Additionally, there are two three-winding transformers with a transformation ratio of 155/33/33 kV and power ratings for each winding of 240/120/120 MVA.

The VSC-HVDC link consists of a rectifier element that converts the power from the wind farm from alternating current to direct current at a voltage level of 150 kV. The DC bus is made up of a 100 km long bipole link. The link culminates with an inverter element that takes power from the DC bus and converts it back to alternating current to be delivered to a transformer, which raises the voltage from 110 kV to 345 kV, corresponding to the voltage of bus 16 (the connection point of the VSC-HVDC link) of the network. This same element contains a control loop that enables the delivery of virtual inertia via the VSC-HVDC link.

Figure 7 displays the configuration of the VSC-HVDC link and its constituent elements, while the connection point with the IEEE 39-bus test system is shown in Figure 6.

Table 1. Generator dispatch parameters of the IEEE 39-bus test system.

Name	Bus Type	Nominal Apparent Power (MVA)	Active Power (MW)	Reactive Power (MVAR)
G 01	PV	10,000	1000	96.89808
G 02	SL	700	217.8205	174.5153
G 03	PV	800	650	215.5386
G 04	PV	800	632	130.7027
G 05	PV	300	508	175.3939
G 06	PV	800	650	235.7521
G 07	PV	700	560	114.4111
G 08	PV	700	540	15.10529
G 09	PV	1000	630	−8.693133
G 10	PV	1000	450	159.7332

Table 2. Nominal values of system loads.

Name	Connection Bus	Active Power (MW)	Reactive Power (MVAR)
LOAD 23	Bus 23	247.5	84.6
LOAD 31	Bus 31	9.2	4.6
LOAD 39	Bus 39	1104	250
LOAD 03	Bus 03	322	2.4
LOAD 04	Bus 04	500	184
LOAD 07	Bus 07	233.8	84
LOAD 08	Bus 08	522	176
LOAD 12	Bus 12	7.5	88
LOAD 15	Bus 15	320	153
LOAD 16	Bus 16	329	32.3
LOAD 18	Bus 18	158	30
LOAD 20	Bus 20	628	103
LOAD 21	Bus 21	274	115
LOAD 24	Bus 24	308.6	−92.2
LOAD 25	Bus 25	224	47.2
LOAD 26	Bus 26	139	17
LOAD 27	Bus 27	281	75.5
LOAD 28	Bus 28	206	27.6
LOAD 29	Bus 29	283.5	26.9

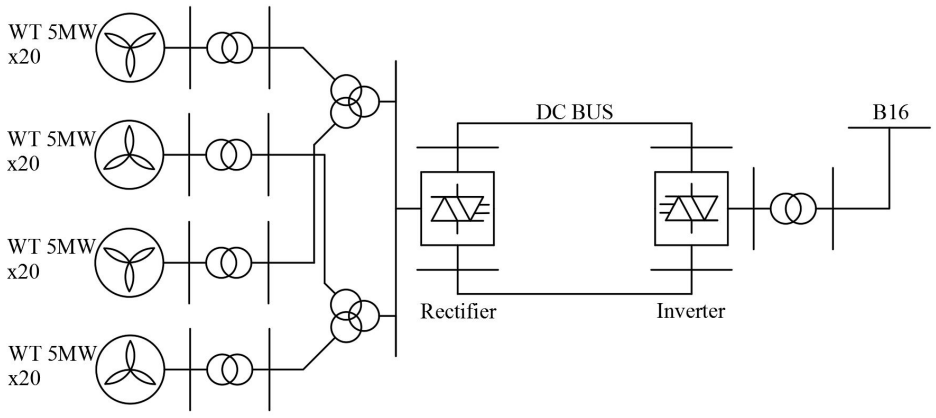

Figure 7. Simplified model of the wind farm and the VSC-HVDC link.

Six cases were considered and analyzed. Each case represents a different frequency response configuration in the event of generation loss, taking into account the presence or absence of a VSC-HVDC link, traditional and optimized UFLS schemes, as well as the injection of virtual inertia by the VSC-HVDC link. These cases were designed to examine and compare the frequency response under different operational instructions, providing a comprehensive insight into how these affect frequency response in power system situations:

- Case 1: Frequency response to generation loss without VSC-HVDC link and UFLS scheme (base case).
- Case 2: Frequency response to generation loss considering VSC-HVDC link operation without virtual inertia injection and without UFLS scheme.
- Case 3: Frequency response to generation loss considering the operation of a traditional UFLS scheme and a VSC-HVDC link without inertia.
- Case 4: Frequency response to generation loss considering the virtual inertia injection of the VSC-HVDC link and the operation of a traditional UFLS.
- Case 5: Frequency response to generation loss considering the operation of an optimized UFLS scheme and a VSC-HVDC link without inertia.
- Case 6: Frequency response to generation loss considering virtual inertia injection of the VSC-HVDC link and operation of an optimized UFLS.

5.1. Case 1

The VSC-HVDC link is considered out of service and therefore does not contribute power to the grid. The UFLS protection scheme is deactivated, while the frequency event is caused by the sudden disconnection of 750 MW dispatched from generator 09. The nadir reached corresponds to 57.85 Hz, with no load shedding, and the frequency value, 10 s after the frequency event (12 s into the simulation) is 58.45 Hz.

In this case, the nadir does not exceed the threshold of 57.5 Hz, which corresponds to the frequency value that should not be exceeded as the lower limit. However, in this scenario, the established metric for the system frequency being above the initial stage of UFLS operation is not met 10 s after the fault or frequency event has occurred. The curve that represents the frequency behavior of case 1 is illustrated in Figure 8.

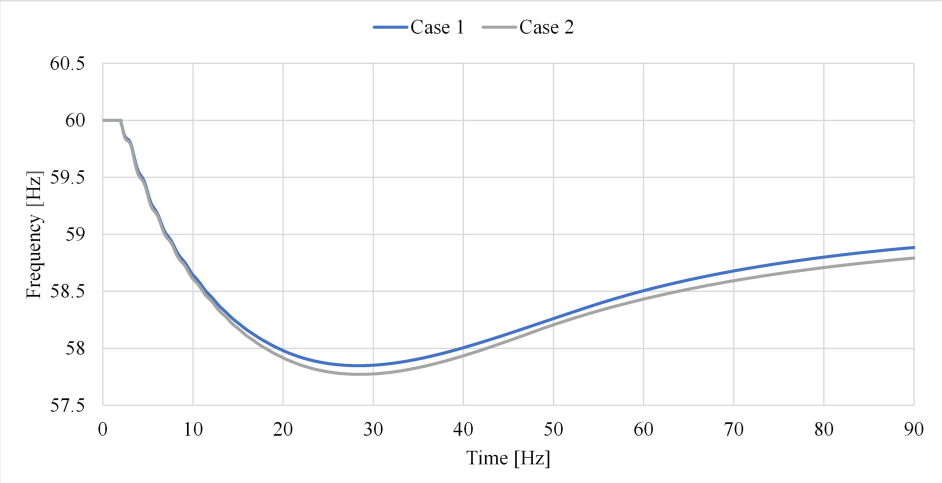

Figure 8. Comparison between the frequency response of cases 1 and 2.

5.2. Case 2

In this case, the injection of 300 MW using the VSC-HVDC link is considered. This power injection displaces the generation present in the grid and the provided spinning inertia. Thus, the overall system inertia decreases, and the frequency nadir increases following the loss of generator G09. The reached nadir corresponds to 57.77 Hz, and the frequency value 10 s after the fault is 58.42 Hz. The frequency metrics show a degradation

in their performance, resulting from the loss of inertia in the system. Figure 8 presents the comparison between the frequency responses resulting from the simulations of cases 1 and 2. In this case, the blue curve corresponds to the frequency obtained in case 1, while the gray curve, below the former, corresponds to the frequency response in case 2. With the injection of inertia power via the VSC-HVDC link, a better frequency response is achieved, resulting in a less pronounced nadir and a closer steady-state operation to the nominal operating frequency.

5.3. Case 3

In this case, the operation of a non-optimized UFLS scheme, referred to as traditional, is considered. A UFLS scheme was programmed with the characteristics presented in Table 3. In this scenario, the VSC-HVDC link is injecting power; however, the inertial response control is deactivated. The UFLS operates and maintains the frequency within the limits and/or operational constraints, namely:

- The frequency will never be less than 57.5 Hz.
- In contingencies, the time that the frequency remains below 58.5 Hz should be minimized.
- After 10 s of an event, the system frequency should be above the threshold of the first stage of the UFLS.
- The amount of load to be disconnected in events should be optimized, avoiding over frequency as much as possible, i.e., frequencies exceeding 60 Hz after an event has occurred.

Table 3. Traditional UFLS parameters.

Stage	Frequency Threshold (Hz)	Load Shedding Percentage (%)	Delay (s)
1	59.4	6.7	0.2
2	59.2	6.7	0.2
3	59	6.7	0.4
4	58.8	6.7	0.4
5	58.6	6.7	0.6
6	58.4	6.7	1

In this case, the reached frequency nadir is 59.31 Hz, resulting in 420.41 MW of load shedding. The frequency behavior results for cases 3, 4, 5 and 6 are presented in Figure 9. Figure 9a illustrates the frequency behavior over 90 s, while Figure 9b highlights the frequency nadir within a 17 s time window.

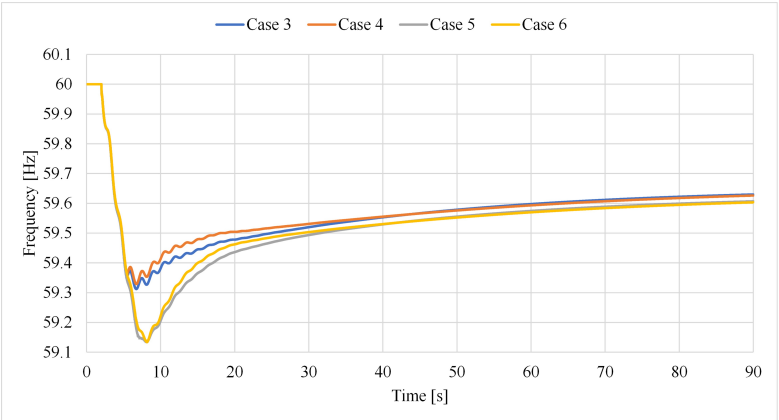

(**a**) Frequency behavior between 0 and 90 s.

Figure 9. *Cont.*

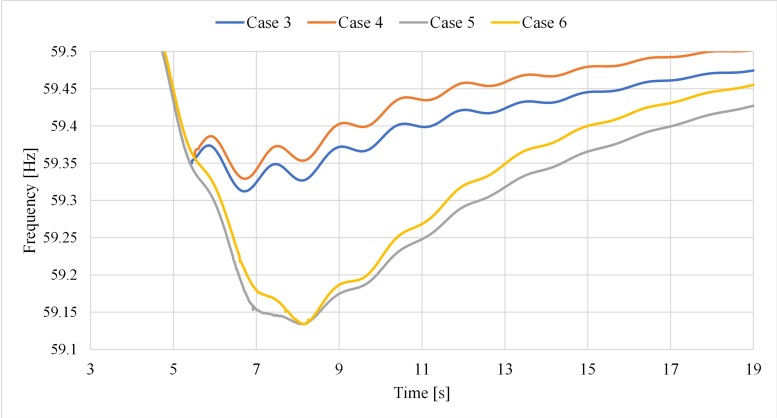

(**b**) Frequency nadir.

Figure 9. Frequency response under generation loss, cases 3, 4, 5 and 6. (**a**) Time window of 90 s. (**b**) Nadir region, range of 17 s between 3 and 19 s of the simulations.

5.4. Case 4

In this case, the operation of the traditional scheme described in case 3 is considered; however, the operation of the VSC-HVDC link considers the injection of virtual inertia. A nadir of 59.33 Hz is reached, with a total shed power of 420.57 MW. With the operation of the control loop that allows the injection of virtual inertia via the VSC-HVDC link, the frequency nadir worsens slightly in case 4 compared to case 3, increasing from 59.31 Hz to 59.33 Hz. This is due to the delay in the activation of some stages of the UFLS scheme caused by the action of virtual inertia.

5.5. Case 5

In this case, the operation of an optimized UFLS scheme and a VSC-HVDC link that does not deliver virtual inertia is considered, as the control loop for this process is deactivated. The operation constraints of the GA are as stated in case 3, and their violations are penalized by increasing the value of the objective function or shed power. Some of the constraints are used to define the search spaces for each of the relay parameter values (activation thresholds and maximum shedding percentages). Additionally, the algorithm considers the device placement by discretizing values between 0 and 1 to determine when the relay is considered on or off. Hence, if the algorithm yields a value between 0 and 0.5, it is considered 0, and the relay is activated. Conversely, if the algorithm produces a value greater than 0.5 and less than or equal to 1, it is considered 1, and the relay is deactivated. The logic of deactivation (1) and activation (0) depends on whether it is out of service (1) or not (0), as employed by the DigSILENT PowerFactory simulation software. Finally, for this case, the reached frequency nadir is 59.13 Hz, with a total shed power of 405.54 MW.

5.6. Case 6

In this case, the operation of the optimized UFLS scheme is considered, along with the injection of inertia power by the VSC-HVDC link. The reached nadir corresponds to 59.13 Hz, with the UFLS shedding a power of 405.67 MW.

When comparing the frequency behavior for cases 5 and 6, it can be observed that the curve corresponding to case 6 shifts to the right compared to the curve of case 5. This is due to the effect of virtual inertia, which allows for reaching the frequency nadir. The frequency nadir reached in both cases is the same when rounded to two decimal places. However, when considering more digits, the nadir corresponding to case 5 (without virtual inertia) exhibits slightly better performance at 59.134092 Hz compared to 59.134001 Hz for case 6.

With the virtual inertia provided by the HVDC VSC link, the frequency drop is expected to be slower. This is because the HVDC VSC control detects the change in ROCOF and takes action to inject power into the system, helping to mitigate the abrupt decrease in

frequency. However, in case 6, where the frequency curve considers the injection of virtual inertia using the HVDC VSC link, a lower nadir is reached because the frequency drop is delayed, thereby causing the a delay in the UFLS scheme to act. Thus, when the HVDC VSC provides virtual inertia, some loads have already been disconnected by the UFLS scheme before the frequency reaches the same level, as it would have otherwise reached without the virtual inertia. This results in a more pronounced decrease in the total demand and, as a consequence, the frequency reaches a slightly higher nadir than in the scenario without virtual inertia.

Figure 10 illustrates a comparison between the load shedding through the UFLS scheme in every study case. It can be seen that in cases 5 and 6, the load shedding is considerably lower compared to the ones in cases 3 and 4. The optimized UFLS scheme ends up approximating the nadir to the constraint value to reduce the load shedding, sacrificing the steady-state frequency value (dependent on the total magnitude of the load shedding).

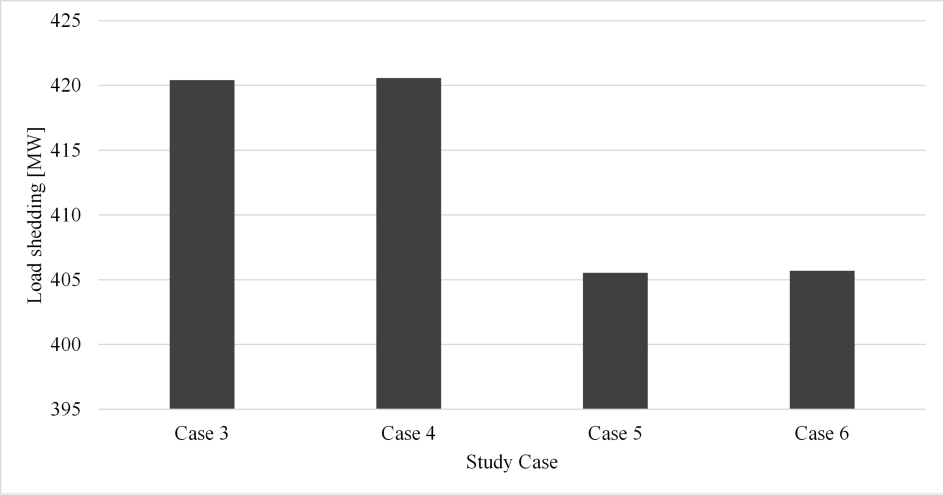

Figure 10. Comparison between load shedding using the UFLS scheme of case studies 3, 4, 5 and 6.

6. Conclusions

In this study, the impact of an under-frequency load shedding (UFLS) scheme and a voltage source converter-based high voltage direct current (VSC-HVDC) link on the frequency response of a power system was evaluated. A comprehensive dynamic simulation model of the power system was developed using DigSILENT PowerFactory. Six operating cases were considered in which the frequency nadir and the total load shedding were analyzed. The following corresponds to the general conclusions of this study: (1) The operation of the UFLS scheme is essential for maintaining the frequency within acceptable limits during under-frequency events. The scheme allows for the shedding of an appropriate amount of load to stabilize the frequency. (2) The provision of synthetic inertia via the VSC-HVDC link can help to improve the frequency response of the power system during under-frequency events. The curves have a lower RoCoF and therefore reach nadir at a later time than those that do not consider virtual inertia injection. (3) The coordination between the UFLS scheme and the VSC-HVDC link is crucial to ensure an effective and optimized frequency response. (4) Synchronization between the controls of both systems can help minimize the impact on the frequency nadir and the overall stability of the power system.

Concerning the cases where an optimization process was implemented, the curves corresponding to the optimized UFLS exhibit a significantly more pronounced nadir with a difference of approximately 0.3 Hz, which does not violate the initially imposed constraints for scheme evaluation. However, the power shed by the optimized UFLS scheme undergoes a significant reduction compared to the traditional UFLS with a difference of approximately 15 MW. Since the steady-state frequency value depends on the balance between the energy

demanded by the load and supplied by the generation, by shedding less load with the optimized UFLS scheme, a lower frequency value is obtained compared to the traditional UFLS scheme.

Author Contributions: Conceptualization, S.B.-M., J.W.G.-S., N.M.-G., S.D.S.-Z. and J.M.L.-L.; Data curation, S.B.-M.; Formal analysis, S.B.-M., J.W.G.-S., N.M.-G., S.D.S.-Z. and J.M.L.-L.; Funding acquisition, J.M.L.-L., J.W.G.-S. and N.M.-G.; Investigation, S.B.-M., J.W.G.-S., N.M.-G., S.D.S.-Z. and J.M.L.-L.; Methodology, S.B.-M., J.W.G.-S., N.M.-G., S.D.S.-Z. and J.M.L.-L.; Project administration, S.D.S.-Z. and N.M.-G.; Resources, S.D.S.-Z., N.M.-G. and J.M.L.-L.; Software, S.B.-M.; Supervision, N.M.-G. and J.M.L.-L.; Validation, S.B.-M.; Test, S.B.-M. and J.W.G.-S.; Visualization, S.B.-M., J.W.G.-S., N.M.-G., S.D.S.-Z. and J.M.L.-L.; Writing—original draft, S.B.-M.; Writing—review and editing, S.B.-M., J.W.G.-S., N.M.-G., S.D.S.-Z. and J.M.L.-L. All authors have read and agreed to the published version of the manuscript.

Funding: This research was funded by Universidad de Antioquia (Medellin, 050010, Colombia) and Institución Universitaria Pascual Bravo (Medellin, 050036, Colombia).

Data Availability Statement: Data is contained within the article and Appendix A.

Acknowledgments: The authors gratefully acknowledge the financial support provided by the Colombian Ministry of Science, Technology, and Innovation "MinCiencias" through "Patrimonio Autónomo Fondo Nacional de Financiamiento para la Ciencia, la Tecnología y la Innovación, Francisco José de Caldas" (Perseo alliance Contract No. 112721-392-2023).

Conflicts of Interest: The authors declare no conflicts of interest.

Appendix A. Parameters of the IEEE 39-Bus Test System

Table A1. IEEE 39-bus test system transmission line parameters.

Name	Bus i	Bus j	R1 (OHM)	X1 (OHM)	Length (km)
LINE 01-02	Bus 01	Bus 02	4.165876	48.91928	163.0643
LINE 01-39	Bus 01	Bus 39	1.19025	29.75625	99.1875
LINE 02-03	Bus 02	Bus 03	1.547325	17.97277	59.90925
LINE 02-25	Bus 02	Bus 25	8.33175	10.23615	34.1205
LINE 03-04	Bus 03	Bus 04	1.547325	25.35233	84.50775
LINE 03-18	Bus 03	Bus 18	1.309275	15.83033	52.76775
LINE 04-05	Bus 04	Bus 05	0.9522001	15.2352	50.784
LINE 04-14	Bus 04	Bus 14	0.9521999	15.35423	51.18075
LINE 05-06	Bus 05	Bus 06	0.23805	3.09465	10.3155
LINE 05-08	Bus 05	Bus 08	0.9521999	13.3308	44.436
LINE 06-07	Bus 06	Bus 07	0.7141501	10.9503	36.501
LINE 06-11	Bus 06	Bus 11	0.8331751	9.760051	32.5335
LINE 07-08	Bus 07	Bus 08	0.4761001	5.47515	18.2505
LINE 08-09	Bus 08	Bus 09	2.737574	43.20608	144.0202
LINE 09-39	Bus 09	Bus 39	1.19025	29.75625	99.1875
LINE 10-11	Bus 10	Bus 11	0.4761001	5.118075	17.06025
LINE 10-13	Bus 10	Bus 13	0.4761001	5.118075	17.06025
LINE 13-14	Bus 13	Bus 14	1.071225	12.02153	40.07175
LINE 14-15	Bus 14	Bus 15	2.14245	25.82843	86.09475
LINE 15-16	Bus 15	Bus 16	1.071225	11.18835	37.2945
LINE 16-17	Bus 16	Bus 17	0.8331751	10.59323	35.31075
LINE 16-19	Bus 16	Bus 19	1.9044	23.20988	77.36625
LINE 16-21	Bus 16	Bus 21	0.9522001	16.06837	53.56125
LINE 16-24	Bus 16	Bus 24	0.3570751	7.022476	23.40825
LINE 17-18	Bus 17	Bus 18	0.8331751	9.760051	32.5335
LINE 17-27	Bus 17	Bus 27	1.547325	20.59133	68.63775
LINE 21-22	Bus 21	Bus 22	0.9522001	16.6635	55.545
LINE 22-23	Bus 22	Bus 23	0.7141501	11.4264	38.088
LINE 23-24	Bus 23	Bus 24	2.61855	41.65875	138.8625
LINE 25-26	Bus 25	Bus 26	3.8088	38.44508	128.1503
LINE 26-27	Bus 26	Bus 27	1.66635	17.49668	58.32225
LINE 26-28	Bus 26	Bus 28	5.118075	56.41785	188.0595
LINE 26-29	Bus 26	Bus 29	6.784425	74.39063	247.9688
LINE 28-29	Bus 28	Bus 29	1.66635	17.97277	59.90925

Table A2. IEEE 39-bus test system transformer parameters.

Name	Nominal Apparent Power (MVA)	Voltage Relation (HV/LV)	Short Circuit Impedance (%)
TRF 02-30	1000	YN 345/16.5 Y	18.1
TRF 06-31	700	YN 345/16.5 Y	17.5
TRF 10-32	800	YN 345/16.5 Y	16
TRF 11-12	300	YN 345/138 Y	13.06
TRF 13-12	300	YN 345/138 Y	13.06
TRF 19-20	1000	YN 345/230 Y	13.82
TRF 19-33	800	YN 345/16.5 Y	11.37
TRF 20-34	300	YN 345/16.5 Y	10.81
TRF 22-35	800	YN 345/16.5 Y	11.44
TRF 23-36	700	YN 345/16.5 Y	19.04
TRF 25-37	700	YN 345/16.5 Y	16.25
TRF 29-38	1000	YN 345/16.5 Y	15.62

References

1. Ebinyu, E.; Abdel-Rahim, O.; Mansour, D.E.A.; Shoyama, M.; Abdelkader, S.M. Grid-Forming Control: Advancements towards 100% Inverter-Based Grids—A Review. *Energies* **2023**, *16*, 7579. [CrossRef]
2. Alavi-Koosha, A.; Amraee, T.; Oskouee, S.S. A multi-area design of under frequency load shedding schemes considering energy storage system. *IET Gener. Transm. Distrib.* **2023**, *17*, 4437–4452. [CrossRef]
3. Schäfer, B.; Beck, C.; Aihara, K.; Witthaut, D.; Timme, M. Non-Gaussian power grid frequency fluctuations characterized by Lévy-stable laws and superstatistics. *Nat. Energy* **2018**, *3*, 119–126. [CrossRef]
4. Seheda, M.S.; Dudurych, O.B. Issues of inertia response and rate of change of frequency in power systems with different penetration of variable speed wind turbines. In Proceedings of the 2016 Electric Power Networks (EPNet), Szklarska Poreba, Poland, 19–21 September 2016; pp. 1–4. [CrossRef]
5. Haes Alhelou, H.; Golshan, M.E.H.; Hatziargyriou, N.D. A Decentralized Functional Observer Based Optimal LFC Considering Unknown Inputs, Uncertainties, and Cyber-Attacks. *IEEE Trans. Power Syst.* **2019**, *34*, 4408–4417. [CrossRef]
6. Acosta, M.N.; Adiyabazar, C.; Gonzalez-Longatt, F.; Andrade, M.A.; Torres, J.R.; Vazquez, E.; Riquelme Santos, J.M. Optimal Under-Frequency Load Shedding Setting at Altai-Uliastai Regional Power System, Mongolia. *Energies* **2020**, *13*, 5390. [CrossRef]
7. Hsu, C.T.; Chuang, H.J.; Chen, C.S. Adaptive load shedding for an industrial petroleum cogeneration system. *Expert Syst. Appl.* **2011**, *38*, 13967–13974. [CrossRef]
8. Hong, Y.Y.; Nguyen, M.T. Multiobjective Multiscenario Under-Frequency Load Shedding in a Standalone Power System. *IEEE Syst. J.* **2020**, *14*, 2759–2769. [CrossRef]
9. Hooshmand, R.; Moazzami, M. Optimal design of adaptive under frequency load shedding using artificial neural networks in isolated power system. *Int. J. Electr. Power Energy Syst.* **2012**, *42*, 220–228. [CrossRef]
10. Rafinia, A.; Moshtagh, J.; Rezaei, N. Stochastic optimal robust design of a new multi-stage under-frequency load shedding system considering renewable energy sources. *Int. J. Electr. Power Energy Syst.* **2020**, *118*, 105735. [CrossRef]
11. Kumar, A.; Thakur, R. A Fuzzy Logic Based Load Shedding Technique for Operation of DG in Islanding Mode. In Proceedings of the 2017 IEEE International Conference on Computational Intelligence and Computing Research (ICCIC), Coimbatore, India, 14–16 December 2017; pp. 1–4. [CrossRef]
12. Haidar, A.M.; Mohamed, A.; Hussain, A. Vulnerability control of large scale interconnected power system using neuro-fuzzy load shedding approach. *Expert Syst. Appl.* **2010**, *37*, 3171–3176. [CrossRef]
13. Talaat, M.; Hatata, A.; Alsayyari, A.S.; Alblawi, A. A smart load management system based on the grasshopper optimization algorithm using the under-frequency load shedding approach. *Energy* **2020**, *190*, 116423. [CrossRef]
14. Amraee, T.; Darebaghi, M.G.; Soroudi, A.; Keane, A. Probabilistic Under Frequency Load Shedding Considering RoCoF Relays of Distributed Generators. *IEEE Trans. Power Syst.* **2018**, *33*, 3587–3598. [CrossRef]
15. Banijamali, S.S.; Amraee, T. Semi-Adaptive Setting of Under Frequency Load Shedding Relays Considering Credible Generation Outage Scenarios. *IEEE Trans. Power Deliv.* **2019**, *34*, 1098–1108. [CrossRef]
16. Badesa, L.; O'Malley, C.; Parajeles, M.; Strbac, G. Chance-constrained allocation of UFLS candidate feeders under high penetration of distributed generation. *Int. J. Electr. Power Energy Syst.* **2023**, *147*, 108782. [CrossRef]
17. Masood, N.A.; Jawad, A.; Banik, S. A RoCoF-constrained underfrequency load shedding scheme with static voltage stability-based zoning approach. *Sustain. Energy Grids Netw.* **2023**, *35*, 101080. [CrossRef]
18. Cai, G.; Zhou, S.; Liu, C.; Zhang, Y.; Guo, S.; Cao, Z. Hierarchical under frequency load shedding scheme for inter-connected power systems. *Prot. Control. Mod. Power Syst.* **2023**, *8*, 34. [CrossRef]
19. Haes Alhelou, H.; Hamedani Golshan, M.E.; Njenda, T.C.; Hatziargyriou, N.D. An Overview of UFLS in Conventional, Modern, and Future Smart Power Systems: Challenges and Opportunities. *Electr. Power Syst. Res.* **2020**, *179*, 106054. [CrossRef]
20. Wang, J.; Zhang, H.; Zhou, Y. Intelligent Under Frequency and Under Voltage Load Shedding Method Based on the Active Participation of Smart Appliances. *IEEE Trans. Smart Grid* **2017**, *8*, 353–361. [CrossRef]

21. Huang, B.; Du, Z.; Liu, Y.; Zhao, F. Study on online under-frequency load shedding strategy with virtual inertia control of wind turbines. *J. Eng.* **2017**, *2017*, 1819–1823. [CrossRef]
22. Gonzalez-Longatt, F.; Chikuni, E.; Stemmet, W.; Folly, K. Effects of the synthetic inertia from wind power on the total system inertia after a frequency disturbance. In Proceedings of the IEEE Power and Energy Society Conference and Exposition in Africa: Intelligent Grid Integration of Renewable Energy Resources (PowerAfrica), Johannesburg, South Africa, 9–13 July 2012; pp. 1–7. [CrossRef]
23. Kundur, P. *Power System Stability and Control*; McGraw-Hill: New Delhi, India, 1994; p. 1167.
24. Johnson, A. System Technical Performance-Simulated Inertia 2010. Available online: https://www.nationalgrideso.com/document/10376/download (accessed on 30 April 2023).
25. Yu, M.; Dyśko, A.; Booth, C.D.; Roscoe, A.J.; Zhu, J. A review of control methods for providing frequency response in VSC-HVDC transmission systems. In Proceedings of the 2014 49th International Universities Power Engineering Conference (UPEC), Cluj-Napoca, Romania, 2–5 September 2014; pp. 1–6. [CrossRef]
26. Zhu, J.; Booth, C.D.; Adam, G.P.; Roscoe, A.J.; Bright, C.G. Inertia Emulation Control Strategy for VSC-HVDC Transmission Systems. *IEEE Trans. Power Syst.* **2013**, *28*, 1277–1287. [CrossRef]
27. Haileselassie, T.M.; Torres-Olguin, R.E.; Vrana, T.K.; Uhlen, K.; Undeland, T. Main grid frequency support strategy for VSC-HVDC connected wind farms with variable speed wind turbines. In Proceedings of the 2011 IEEE Trondheim PowerTech, Trondheim, Norway, 19–23 June 2011. [CrossRef]
28. Li, Y.; Zhang, Z.; Yang, Y.; Li, Y.; Chen, H.; Xu, Z. Coordinated control of wind farm and VSC-HVDC system using capacitor energy and kinetic energy to improve inertia level of power systems. *Int. J. Electr. Power Energy Syst.* **2014**, *59*, 79–92. [CrossRef]
29. Pérez Posada, A.F.; Villegas, J.G.; López-Lezama, J.M. A Scatter Search Heuristic for the Optimal Location, Sizing and Contract Pricing of Distributed Generation in Electric Distribution Systems. *Energies* **2017**, *10*, 1449. [CrossRef]
30. Sanin-Villa, D.; Montoya, O.D.; Grisales-Noreña, L.F. Material Property Characterization and Parameter Estimation of Thermoelectric Generator by Using a Master—Slave Strategy Based on Metaheuristics Techniques. *Mathematics* **2023**, *11*, 1326. [CrossRef]
31. Swaminathan, D.; Rajagopalan, A.; Montoya, O.D.; Arul, S.; Grisales-Noreña, L.F. Distribution Network Reconfiguration Based on Hybrid Golden Flower Algorithm for Smart Cities Evolution. *Energies* **2023**, *16*, 2454. [CrossRef]
32. Agudelo, L.; López-Lezama, J.M.; Muñoz-Galeano, N. Vulnerability assessment of power systems to intentional attacks using a specialized genetic algorithm. *Dyna* **2015**, *82*, 78–84. [CrossRef]
33. Almazrouei, O.S.M.B.H.; Magalingam, P.; Hasan, M.K.; Shanmugam, M. A Review on Attack Graph Analysis for IoT Vulnerability Assessment: Challenges, Open Issues, and Future Directions. *IEEE Access* **2023**, *11*, 44350–44376. [CrossRef]
34. Saldarriaga-Zuluaga, S.D.; López-Lezama, J.M.; Muñoz-Galeano, N. Adaptive protection coordination scheme in microgrids using directional over-current relays with non-standard characteristics. *Heliyon* **2021**, *7*, e06665. [CrossRef]
35. Castillo Salazar, C.A.; Conde Enriquez, A. Coordination of Overcurrent Relays Using Genetic Algorithms and Unconventional Curves. *IEEE Lat. Am. Trans.* **2014**, *12*, 1449–1455. [CrossRef]
36. Jiménez, J.; Guardado, J.L.; Cabrera, N.G.; Rodriguez, J.R.; Figueroa, F. Transmission expansion planning systems using algorithm genetic with multi-objective criterion. *IEEE Lat. Am. Trans.* **2017**, *15*, 563–568. [CrossRef]
37. Huamannahui Huanca, D.; Gallego Pareja, L.A. Chu and Beasley Genetic Algorithm to Solve the Transmission Network Expansion Planning Problem Considering Active Power Losses. *IEEE Lat. Am. Trans.* **2021**, *19*, 1967–1975. [CrossRef]
38. Hong, Y.Y.; Wei, S.F. Multiobjective underfrequency load shedding in an autonomous system using hierarchical genetic algorithms. *IEEE Trans. Power Deliv.* **2010**, *25*, 1355–1362. [CrossRef]
39. Sanaye-Pasand, M.; Davarpanah, M. A new adaptive multidimensioanal load shedding scheme using genetic algorithm. In Proceedings of the 2005 Canadian Conference on Electrical and Computer Engineering, Saskatoon, SK, Canada, 1–4 May 2005; pp. 1974–1977. [CrossRef]
40. Fan, Y.; Zi, X.; Jun, L.; Bingbing, L. Research on optimal load shedding for active distribution network based on genetic algorithm. In Proceedings of the 2017 2nd International Conference on Power and Renewable Energy, ICPRE 2017, Chengdu, China, 20–23 September 2017; pp. 510–514. [CrossRef]
41. Saldarriaga-Zuluaga, S.D.; López-Lezama, J.M.; Muñoz-Galeano, N. Optimal coordination of overcurrent relays in microgrids considering a non-standard characteristic. *Energies* **2020**, *13*, 922. [CrossRef]
42. Wu, X.; Xue, F.; Dai, J.; Tang, Y. Adaptive Under-Frequency Load Shedding Control Strategy of Power Systems With Wind Turbines and UHVDC Participating in Frequency Regulation. *Front. Energy Res.* **2022**, *10*, 875785. [CrossRef]
43. Tang, G.; Xu, Z.; Dong, H.; Xu, Q. Sliding Mode Robust Control Based Active-Power Modulation of Multi-Terminal HVDC Transmissions. *IEEE Trans. Power Syst.* **2016**, *31*, 1614–1623. [CrossRef]
44. Zhang, H.; Zhang, Y. Research on interval multi-objective optimal power flow in AC-DC systems considering wind power fluctuation. *Wind Eng.* **2021**, *45*, 1587–1600. [CrossRef]
45. Xiao, L.; Xu, Z.; Xiao, H.; Zhang, Z.; Wang, G.; Xu, Y. Electro-mechanical transient modeling of MMC based multi-terminal HVDC system with DC faults considered. *Int. J. Electr. Power Energy Syst.* **2019**, *113*, 1002–1013. [CrossRef]

46. Tan, B.; Zhao, J.; Duan, N.; Maldonado, D.A.; Zhang, Y.; Zhang, H.; Anitescu, M. Distributed Frequency Divider for Power System Bus Frequency Online Estimation Considering Virtual Inertia From DFIGs. *IEEE J. Emerg. Sel. Top. Circuits Syst.* **2022**, *12*, 161–171. [CrossRef]
47. Abu Talib, D.N.; Mokhlis, H.; Abu Talip, M.S.; Naidu, K.; Suyono, H. Power System Restoration Planning Strategy Based on Optimal Energizing Time of Sectionalizing Islands. *Energies* **2018**, *11*, 1316. [CrossRef]

Disclaimer/Publisher's Note: The statements, opinions and data contained in all publications are solely those of the individual author(s) and contributor(s) and not of MDPI and/or the editor(s). MDPI and/or the editor(s) disclaim responsibility for any injury to people or property resulting from any ideas, methods, instructions or products referred to in the content.